Magnesium Technology 2013
Edited by: Norbert Hort, Suveen N. Mathaudhu, Neale R. Neelameggham, and Martyn Alderman
TMS (The Minerals, Metals & Materials Society), 2013

A Multi-stage Approach for Predicting Fatigue Damage in Friction Stir Spot Welded Joints of Mg AZ31 Alloy

H.M. Rao[1] and J.B. Jordon[1]
[1]The University of Alabama, Dept. of Mechanical Engineering, Tuscaloosa, AL, 35487

Keywords: Friction Stir Spot Welding, Mg AZ31, Multi Stage Fatigue Modeling

Abstract

In this work, we propose a model for predicting fatigue damage in friction stir spot welded (FSSW) joints made of Mg AZ31 alloy. In this modeling approach, an attempt is made to capture failure mechanisms due to the influence of variation in welding parameters including tool plunge depth, tool rotation speed, and tool pin diameter. As such, the fatigue model presented here is a deterministic approach, where fatigue lifetimes are estimated based on specific geometrical and microstructural information. In particular, the model addresses the observed variation in failure mechanisms commonly observed in Mg FSSW coupons under a range of applied loading. Further, a distinction is made between fatigue crack incubation, microstructural small and physically small fatigue crack growth, and finally long crack growth of the coupon. The fatigue model presented here showed good correlation for fatigue lifetimes for variation in welding conditions.

Introduction

In order to meet and exceed federal standards regarding fuel economy, the automotive industry is exploring lightweight designs. Lightweight metals, such as magnesium alloys, provide substantial weight savings over traditional structure metals, i.e. steels. However, industrial joining techniques for magnesium alloys are not well established compared to more established metals and this is especially true for spot joining. One possible alternative spot joining technology is friction stir spot welding. Friction stir spot welding (FSSW) is a variant of friction stir welding (FSW) and is an attractive spot welding technique due to its solid state process and its low energy requirements.

FSSW is a thermo-mechanical process for spot lap-joing of sheet [1,2] and Fig. 1 shows a schematic of the process. The rotating tool comprises a probe pin that is plunged into two sheets of metal to be joined. The probe pin typically penetrates the upper sheet completely and then passes into the bottom sheet to various depths depending on process conditions. Here, the downward force and rotational speed of the tool generates localized friction as the pin interacts with the upper sheet. The heat generated by friction softens the sheet materials adjacent to the tool and deforms plastically to form a solid state bond between the surface of upper and bottom sheet [3]. A longer dwell period typically provides the driving force for the upwards displacement of lower sheet material which promotes good bonding [2]. Since the dwell time in a manufacturing setting is relatively short, e.g., 2 to 5 seconds, the tool rotation speed and plunging motion largely determines the heat generation [4], joint formation and weld mechanical properties [5]. In general, FSSW is free of defects commonly associated with fusion welding, largely because the temperature attained during FSSW is less than the melting point of base materials. The other advantages of FSSW include no need of cooling agent, filler materials, or post weld treatment. In addition, FSSW is more energy efficient and clean when compared to other types of spot welding techniques.

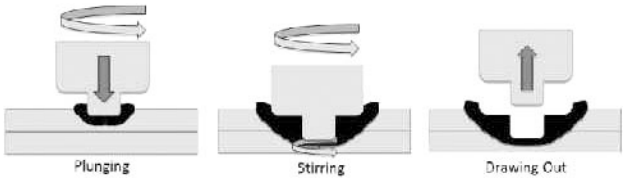

Figure 1. A schematic illustrating the friction stir spot welding process.

While fundamental relationships governing the static strength of FSSW in magnesium alloys have been investigated, only a few studies exist regarding fatigue behavior and performance in Mg alloys [8-10]. In fact, Rao and Jordon [10] analyzed the influence of microstructural and geometrical features on fatigue lifetimes of FSSW on AZ31 Mg alloy. Fractography analysis conducted in this study suggested that the effective top sheet thickness largely determined the failure mode, which in turn influenced the final number of cycles to failure. While the height of the interfacial hook was greater in the process with better fatigue performance, it was the larger effective top sheet thickness that promoted crack propagation modes more favorable to greater fatigue resistance. Furthermore, scanning electron microscopy (SEM) of striation spacing confirmed differences in crack growth rates.

The current state of fatigue modeling of spot welds is successful in correlating the number of cycles to failure for various types of joining methods. The most common approaches use some variation of linear elastic fracture mechanics (LEFM), where the variation in methods is on the determination of the stress intensity solution. However, a deterministic approach to correlate fatigue lifetimes based on specific microstructure and geometrical features of a specific welding process does not currently exist. As such, the purpose of this paper is to establish a microstructure sensitive fatigue model for FSSW joints in Mg alloys. The premise of this model is to capture the classical defined stages of fatigue: incubation; microstructurally small/ physically small crack growth; and long crack growth. To the best of the authors' knowledge, this type of approach has not been applied for FSSW or other similar spot welds.

Materials and Experiments

In order to provide the foundation for the develop of a multi-stage model for FSSW in Mg alloys, results from a recent study [10] and are summarized here. Two sets of FSSW coupons, made using 2.0 mm thick AZ31 Mg alloy sheets, were welded in an overlap configuration. For process #1, the individual sheet dimensions were: length of 100 mm, width of 35mm, and a welded overlap area of 35 x 35 mm. For process #2, the

individual sheet dimensions were: length of 100 mm, width of 38 mm and a welded overlap area of 38 x 38 mm. For process #1, the FSSW tool was made from standard tool steel (H13) material with a shoulder diameter of 12mm and a cylindrical pin having a diameter of 5 mm, pin length of 3.2 mm, and left hand threads (M5), as shown in Fig. 2a. For process #2, the FSSW tool is identical to the tool used in process #1; however the tool had a triangular pin as shown in Fig. 2b. Both tools had a 10° concave shoulder as shown in Fig. 2c.

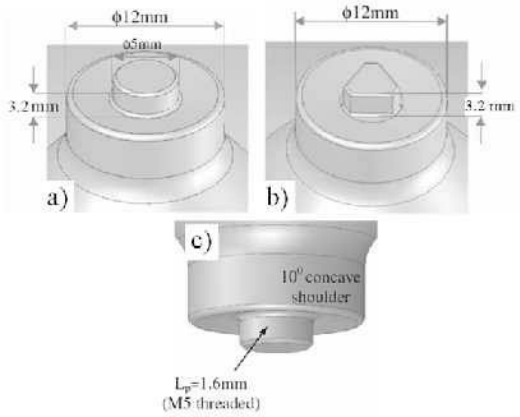

Figure 2. Schematic of the FSSW tool geometry employed for (a) process #1 and (b) process #2.

Table I. lists the process conditions used to join the two sets of lap-shear coupons employed in this study. Figure 3 shows representative lap-shear samples from both process #1 and #2. For the fatigue tests, the lap-shear coupons were cyclically tested in an MTS 810 servo-hydraulic load frame under load control with a sinusoidal waveform at three different load ratios (0.1, 0.3, and 0.7). The fatigue tests were tested at frequencies that ranged from 5–30 Hz. While most of the tests were conducted at 10 Hz, higher frequencies were employed for the low load amplitudes to expedite failure. Steel shims were employed in the test frame to prevent additional bending forces. The grip-to-grip distance employed for each coupon was 110 mm.

Table I. FSSW welding process parameters used in current study.

Welding Parameters	Process #1	Process #2
Tool rotation (RPM)	1000	750
Tool Plunge Speed (mm/min)	20	20
Shoulder Plunge Depth (mm)	0.5	0.1
Dwell Time (sec)	2.5	2.5

For weld characterization, samples were sectioned through the center of the weld nugget coupon and parallel to the loading direction. Samples were cold mounted in epoxy and then ground and polished. Using a Keyence VHX-1000 digital optical microscope, key features of the weld were characterized including size and shape of the interfacial hook, the bond width, and effective sheet thickness. Representative fatigued coupons from process #1 and process #2 were also observed under the Keyence microscope to identify the failure modes at different cyclic load levels.

Interfacial Hooks

In typical FSSW joints, the faying surface oftentimes exhibits a hook-like shape as shown in Fig. 3. This hooking of the faying surface is a result of trapped oxide films are that displaced upward due to the plastic flow of the material resulting from the downward plunge of the pin into the bottom sheet. In fact, the degree of oxide distribution at the faying surface is greatly influenced by the tool geometry and tool rotation speed.

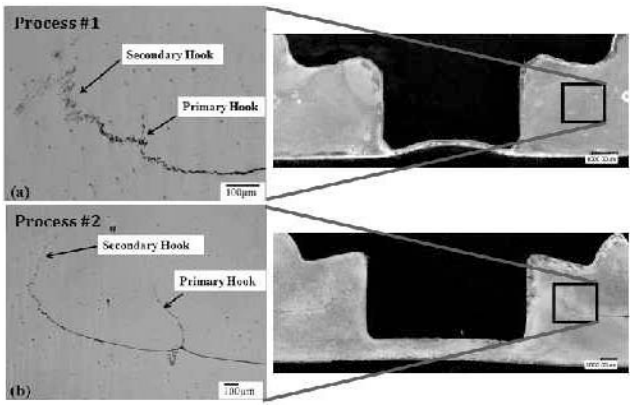

Figure 3. Magnified views of the primary and secondary hooks formed in (a) process #1 and (b) process #2.

Consequently, the link between the sheet thickness, T (see Fig. 4), and hook height are directly related to the shoulder plunge depth achieved during FSSW. If the tip-to-tip distance of the primary interfacial hooks is used to define the bond width, D2 (refer Fig.4), process #2 had a slightly larger bond width. Dimension nomenclature of the various weld geometry measured are indicated in Fig. 4 and the quantified results are shown in Table II.

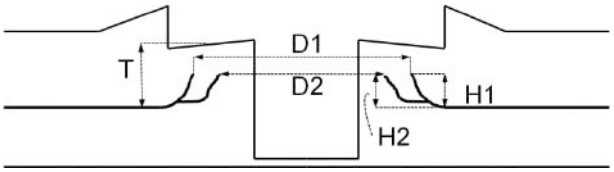

Figure 4. Schematic of key geometrical features of FSSW coupon with dimension nomenclature. (Refer to Table II for dimensions)

Table II. Summary of dimensions of the FSSW features for process #1 and process #2 (refer Figure 5. for nomenclature).

Nomenclature	Process #1 (mm)	Process #2 (mm)
D1	10.8	11.0
D2	10.6	9.5
H1	0.15	0.63
H2	0.28	1.04
T	1.20	1.90

Optical Fractography

Figure 5 shows an overview of representative fractured FSSW coupons from both process #1 and #2. Several macroscale observations were made regarding the failure modes. It can be seen that the dominant crack originated from the interfacial hooks in coupons from the two processes. The mode of failure varied from nugget pullout, top sheet pullout, nugget shear failure and bottom sheet pullout for different loading conditions in the FSSW coupons of the two processes. Table III summarizes the failure modes for the FSSW Mg AZ31 coupons subjected to cyclic

loading for both process #1 and process #2 based on the optical fractography conducted in this study.

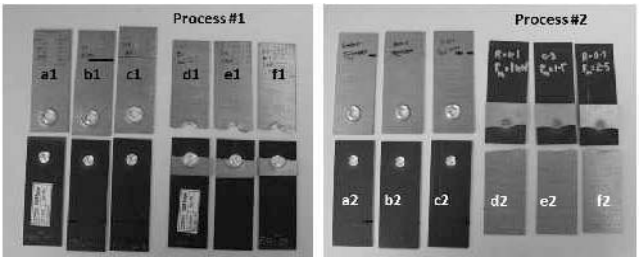

Figure 5. Representative fractured coupons tested at a range of maximum cyclic loads of 1-3 kN at R=0.1, 0.3, and 0.7 (Refer to Table III for a summary of failure modes).

Table III. Summary of failure modes in coupons of process #1 and process #2 (ID correlates with specimens shown in Figure. 5).

Process#1: Mode A (Low Cycle Fatigue Regime)	Dominant crack grew from primary hook into the top sheet, then halfway around the outer circumference of the nugget, finally failing by nugget pullout.
Process#1: Mode B (High Cycle Fatigue Regime)	Dominant crack grew from primary hook into the top sheet, halfway around the outer nugget circumference and then along the width of the top sheet.
Process#2: Mode C (Low Cycle Fatigue Regime)	Dominant crack grew across the weld nugget and parallel to loading direction in mode II propagation.
Process#2: Mode D (High Cycle Fatigue Regime)	The Dominant crack grew from root of the secondary hook into the bottom sheet, propagated around the outer circumference of the nugget region and then along the width of the bottom sheet.

Multi Stage Fatigue Modeling

The multistage fatigue (MSF) model is a microstructure-sensitive model that considers the various experimentally observed stages of fatigue damage evolution such as crack incubation, microstructurally small crack (MSC), physically small crack (PSC), and long crack growth [11]. While the model was originally developed for a cast A356 Al alloy, it has been modified to extend its application to other materials and other processing methods (e.g. processing of wrought materials) [12]. The MSF model is based on three distinct stages of fatigue damage, where total fatigue life N_{Total} is given by

$$N_{Total} = N_{Inc} + N_{MSC/PSC} + N_{LC} \quad (1)$$

where N_{Inc} is the number of cycles to incubate a crack near or at a micro-notch that includes the nucleation of crack-like damage and early crack propagation through the zone of the micronotch's root influence [11]. The $N_{MSC/PSC}$ term is the number of cycles required for propagation of a microstructurally small crack (MSC) and physically small crack (PSC), and N_{LC} is the number of cycles required for long crack propagation.

Crack incubation involves nucleation plus small crack growth at the micronotch of the order of ½ D, where D is the micronotch size. Small crack growth (MSC) comprises propagation of microstructural cracks with lengths that fall within $a_i < a < k\,MS$, where MS is a characteristic length scale (defined as the smallest grain size) of interaction with microstructural (MS) features, and k is a multiplier where $1 \le k \le 3$ [11, 12]. The PSC range consists of crack propagation with a crack length in the interval of $k\,MS < a <\sim 10\,MS$). Depending on the micronotch and texture of the matrix, the PSC regime may extend from 300 μm to ~2-3 mm in length.

Crack Incubation Regime

The fatigue damage incubation life, N_{inc} is characterized by the cyclic damage at the micronotch root and takes on a modified Coffin-Manson law form [11] in the microscale as follows:

$$C_{\text{inc}} N_{\text{inc}}^{\alpha} = \beta = \frac{\Delta\gamma_{max}{}^{p^*}}{2} \quad (2)$$

where β is the nonlocal damage parameter around a micronotch, and C_{inc} and α represent the linear coefficient and exponent, respectively in a modified Coffin-Mason approach for the fatigue crack incubation life. The numerical value of the exponent α was selected to be in the range of the macroscopic Coffin-Mason law [11, 12]. The coefficient in the Coffin-Manson equation, $C_{\text{inc}} = c_n + z(c_m - c_n)$, is modified [11] to include a coefficient for nucleation of small cracks at micronotch in the high cycle regime (c_n) and a coefficient for the low cycle regime (c_m). We further note that $z = (1/0.7)\langle\frac{l}{D} - 0.3\rangle$ is a localization multiplier [11] that is nonzero below the microplasticity percolation limit. Just beyond the percolation limit, the localization multiplier transitions to unity as the plastic shear strain localizes interdendritically [11]. Above that point, incubation is negligible because of the high strain level that localizes at the micronotch [11]. Note that the ratio $\frac{l}{D} = \sqrt{\frac{A_{plastic\,zone}}{A_{notchroot}}}$ is defined as the square root of the ratio of the plastic zone over the micronotch root area. We further note that $\frac{l}{D}$ ratio is typically determined through micro-mechanical simulations. In this study, however, no such simulations were available, and as such, C_{inc} is assumed to be constant for both the high cycle and low cycle regime. The β parameter is related to the local average maximum plastic shear strain amplitude, $\frac{\Delta\gamma_{max}{}^{p^*}}{2}$, and is estimated by the following relations:

$$\beta = \frac{\Delta\gamma_{max}{}^{p^*}}{2} = Y100[\varepsilon_a - 0.00025(1-R)]^X \quad (3)$$

Here, ε_a is the remote applied strain amplitude, the parameter Y [12] is correlated as $Y = y_1 + (1+R)y_2$, where R is the load ratio, and $y_1, y_{2,X}$ are model constants. For completely reversed loading cases, $Y = y_1$.

Small Crack Growth

Similar to modeling efforts in wrought aluminum alloys [12], we combine the mathematical expressions for the MSC and PSC regimes into a single mathematical form. Crack growth in the MSC/PSC is governed by the range of crack tip displacement, ΔCTD, which is proportional to the crack length, and the nth

power of the applied stress amplitude, $\sigma^n{}_a$, in the high cycle fatigue (HCF) regime and to the macroscopic plastic shear strain range, $\frac{\Delta\gamma^P_{max}}{2}$, in the low cycle fatigue (LCF), and it is given by the following,

$$\left(\frac{da}{dN}\right)_{MSC} = \chi(\Delta CTD - \Delta CTD_{th}), \quad (4)$$

$$\Delta CTD = C_{II}\left(\frac{GS}{GS_0}\right)^{\omega}\left[\frac{U\Delta\hat{\sigma}}{S_{ut}}\right]^{\zeta} a_i + C_I\left(\frac{GS}{GS_0}\right)^{\omega}\left(\frac{\Delta\gamma^P_{max}}{2}\right)^2 \quad (5)$$

Here, χ is a constant for a given microstructure, typically less than unity and usually taken as 0.32 for several different alloys [12], and a_i is the initial crack length. The C_I and C_{II}, and ζ are material dependent parameters which capture the microstructural effects on MSC growth [11, 12]. The threshold value for crack tip displacement was defined on the order of the Burger's vector for the Mg-rich matrix [14], $\Delta CTD_{th} = 3.2 * 10^{-4}\mu m$. The term $\Delta\hat{\sigma}$ is the combination of the uniaxial effective stress amplitude, $\bar{\sigma}_a = \sqrt{\frac{3}{2}\frac{\Delta\sigma'_{ij}}{2}\frac{\Delta\sigma'_{ij}}{2}}$, and the maximum principal stress range, $\Delta\sigma_1$, and is given as $\Delta\hat{\sigma} = 2\theta\bar{\sigma}_a + (1-\theta)\Delta\sigma_1$, with $0 \le \theta \le 1$ as the path dependent loading parameter after [12], where θ is a weighting parameter such that $\theta = 0$ gives the von Mises stress state, and $\theta = 1$ gives the maximum for principal stress state. The parameter U is employed to capture the load ratio effects and is defined as $U = \frac{1}{1-R}$ [12]. In order to capture the effect of grain size on small crack growth, we employ the ratio of grain size to the reference size $\left(\frac{GS}{GS_0}\right)^{\omega}$ for each of the three materials in this study, where GS_0 is the reference grain size, GS is the specific grain size, and ω is a material parameter [12].

Long Crack Growth

Linear elastic fracture mechanics is used to model long crack growth in the FSSW coupons. The general expression of the number of cycles were calculated using the relation

$$\left(\frac{da}{dN}\right)_{LC} = C((\Delta K)^M - (\Delta K_{th})^M) \quad (6)$$

where for Mg AZ31, $M \sim 3.68$ and $C \sim 3$ x10^{-10} [15] and the intrinsic threshold is given by $\Delta K_{th} \sim 0.91$ MPa$\sqrt{m}$ for Mg AZ31 [16], as determined from the threshold for long cracks with grains in longitudinal direction. We assume the long crack grows once the MSC/PSC reaches the free surface of the coupon and/or a threshold length of 2mm. Since final separation of the joint in the high cycle fatigue (HCF) regime for both processes occurs through the sheet and not the weld, we assume the following stress intensity solution [17]:

$$K_{eff} = \sigma\sqrt{\pi a}.F\left(\frac{a}{b}\right) \quad (7)$$

where σ is the applied stress, a is the crack length at full separation, b is half the width of the specimen. For process#1 and process#2 in the low cycle fatigue (LCF) regime, the coupons failed due to shear overload in the nugget. Based on work of Jordon et al. [9] for FSSW joints in Mg AZ31 alloy, the following relation is used to estimate the crack growth rate in LCF:

$$K_I = \frac{P}{r^{1.5}}\left[0.314\left(\frac{2r}{t}\right)^{0.397}\right] \quad (8)$$

$$K_{II} = \frac{P}{r^{1.5}}\left[0.282 + 0.162\left(\frac{2r}{t}\right)^{0.710}\right] \quad (9)$$

$$K_{eff} = \sqrt{\left({K_I}^2 + {K_{II}}^2\right)} \quad (10)$$

Where K_I and K_{II} are global stress intensity solutions, P is the load (N), r is the radius of the weld and t is the thickness of the sheet. Table IV (Appendix) lists the MSF model parameters employed in this study.

Modeling Results and Discussion

The MSF model used in this current study for the FSSW joints is an adaptation from the model developed for base materials. The modifications and assumptions were made to closely relate conditions in the FSSW joints that were experimentally observed in [10]. Figure 6 shows the correlation of the MSF model to the experimental load-life results for the FSSW Mg AZ31 alloy for the two sets of processes. It is important to note that the model correlated to the distinct failure modes as listed in Table III. Furthermore, the MSF employed the three distinct stages of fatigue damage: incubation, small crack (MSC/PSC)) and long crack growth (LC) to capture the long crack growth.

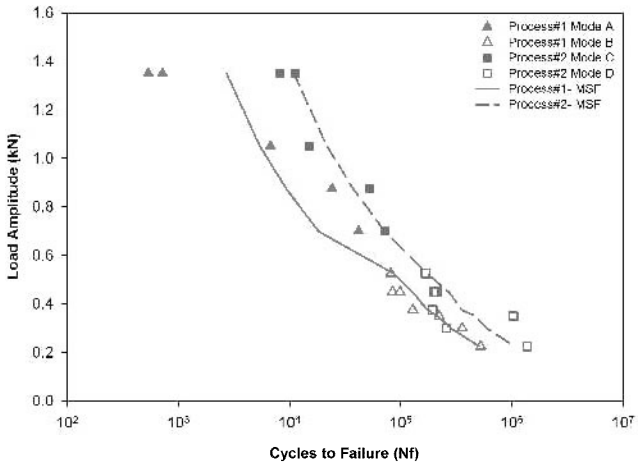

Figure 6. A comparison of experimental fatigue life results with crack growth model prediction of fatigue life of FSSW Mg AZ31 alloy.

The primary inputs to the model include the load amplitude, load ratio, weld geometry such as the hook height and weld radius. The remaining constants are based on assumptions and micromechanical simulations and other accepted values pertaining to microstructure used prior MSF work [11-13]. However, we note that future work is needed to validate some of the model parameters, in particularly the incubation and small crack growth parameters. In fact, as mentioned earlier, micromechanical simulations are planned to validate the parameters employed in this study. However, the results of the MSF correlation to the experimental results suggest that the model framework is well adapted to predicting the fatigue damage in FSSW joints.

Figure 7 and 8 show the contribution of incubation, small crack growth and long crack growth for process #1 and process #2, respectively. As shown in Fig. 7 and Fig. 8 the MSC/PSC is the dominant stage in both the processes in the LCF conditions,

whereas the crack incubation cycle is negligible in both of the process for LCF and HCF. This trend correlates with the experimentally observed conditions of crack propagation dominated damage [10] as compared to some base materials where total fatigue is dominated by incubation [11]. In FSSW, the notch root at the faying surface promotes a short incubate life and thus the majority of total life is spent in internal crack propagation.

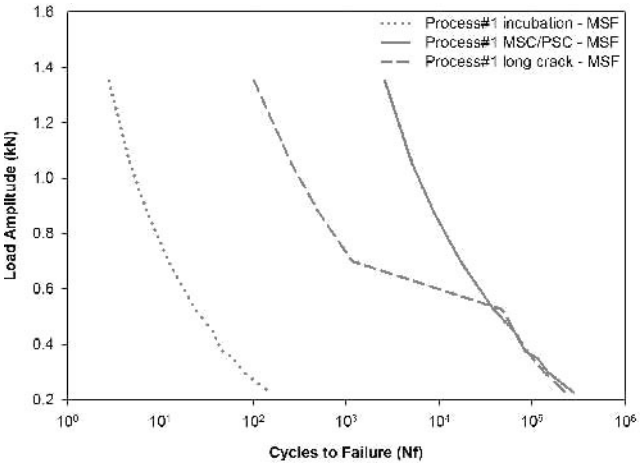

Figure 7. Crack life cycles as predicted by the fatigue model in process#1 under different loading conditions.

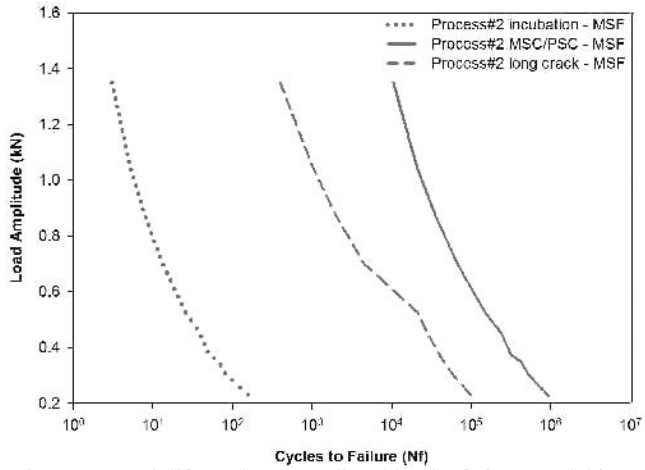

Figure 8. Crack life cycles as predicted by the fatigue model in process#1 under different loading conditions.

Experimentally, we observed that the MSC/PSC propagated through the primary interfacial hook in coupons from process #1, which is in thermomechanically affected zone of the weldment. This region of the weldment is characterized by larger grains which has the least resistance to crack growth. In coupons from process #2, the crack propagated through the root of the secondary hook and traversed to the bottom sheet in the stir zone of the weldment which is characterized by finer recrystalized grains [9, 10]. This crack growth regime contributed to ~ 94% of the total life of the coupons from process #1in LCF and ~ 50% of the total life in HCF. In coupons from process #2, the MSC/PSC contributed to ~ 95% of the total life in LCF and ~ 89% in HCF. This trend indicates that in LCF, the microstructure of the weldment does not contribute much to crack growth resistance and final failure. However, in HCF, the microstructure of the weldment is more crucial in resisting the crack growth and thus as has more of an effect on the final number of cycles as compared to the LCF regime.

Once the MSC/PSC reached the surface of the top sheet in process #1 and bottom sheet in process #2 in HCF, the crack grew along the width of the respective sheet. This growth along the width of the sheets is assumed to be the long crack regime for the fatigue modeling purpose. The long crack growth in process #1 contributed to about ~ 50% of the total life and ~ 11% of the total life in coupons from process #2 in the HCF as predicted by the MSF model. In process #1, the long crack negotiated through the nugget surface and along the width of the top sheet. The grain structure of the nugget and top sheet may contribute to the inhabitation of the growth of the crack. As in coupons from process #2, the long crack propagated in the bottom sheet away from the weld nugget which is not exposed to high physical deformation by the welding process. Hence the grains in this region of the coupon are not recrystalized and do not inhibit crack growth. For coupons in process #1 and process #2 in LCF, the long crack regime contributed to ~ 6% of the total life in process#1 and ~ 11% of the total life in coupons from process #2. Under high loads, the shear stresses are large enough for the long crack to grow through the weld nugget. The MSC/PSC and long crack together constitute to the final shear failure of the nugget in coupons from both the process.

Conclusions

In this paper, we present the formulation of a multi-stage fatigue (MSF) model for friction stir spot welding in Mg alloy. This model not previously applied to joints, was adapted to the lap-shear spot welded coupon to capture the incubation, small crack, and long crack growth stages observed experimentally. In general the MSF model showed good correlation to experimental results. In particular, the model correlated the differences in process conditions employed in fabricating the lap-shear coupons and their effect on the number of cycles to failure. This is a significant development since the results presented here suggest that the MSF model can be used to help elucidate the effect of a particular welding process and loading condition on fatigue lifetimes and help design future friction stir welds based on fatigue requirements.

References

1. S.M. Chowdhurya, D.L. Chena, S.D. Bholea, and X. Caob, "Tensile Properties of a Friction Stir Welded Magnesium Alloy: Effect of Pin Tool Thread Orientation and Weld Pitch," *Materials Science and Engineering A*, 527 (2010), 6064–6075.

2. Y.H. Yin, N. Sunb, T.H. North, and S.S. Hu, "Hook Formation and Mechanical Properties in AZ31 Friction Stir Spot Welds," *Journal of Materials Processing Technology,* 210 (2010), 2062–2070.

3. D.A. Wang, and C.H. Chen, "Fatigue Lives of Friction Stir Spot Welds in Aluminum 6061-T6 Sheets," *Journal of Materials Processing Technology,* 209 (2009), 367-375.

4. A. Gerlich, P. Su, and T.H. North, "Tool Penetration During Friction Stir Spot Welding of Al and Mg Alloys," *Journal of Materials Science*, 40 (2005), 6473–6481.

5. Y.H. Yin, A. Ikuta, and T.H. North, "Microstructural Features and Mechanical Properties of AM60 and AZ31 Friction Stir Spot Welds," *Materials and Design,* 31 (2010), 4764–4776.

6. N. Sun, Y.H. Yin, A.P. Gerlich, and T.H. North, "Tool Design and Stir Zone Grain Size in AZ31 Friction Stir Spot Welds," *Science and Technology of Welding and Joining,* 14 (2009), 747-752.

7. Y.H. Yin, N. Sun, T.H. North, and S.S. Hu, "Influence of Tool Design on Mechanical Properties of AZ31 Friction Stir Spot Welds," *Science and Technology of Welding and Joining,* 15 (2010), 81-86.

8. P.K. Mallick, and L. Agarwal, "Fatigue of Spot Friction Welded Joints of Mg-Mg, Al-Al and Al-Mg Alloys," (Paper presented at Society of Automotive Engineers, Warrendale, PA, 2009), 01-0024.

9. J.B. Jordon, M.F. Horstemeyer, S.R. Daniewicz, H. Badarinarayan, and J. Grantham, "Fatigue Characterization and Modeling of Friction Stir Spot Welds in Magnesium AZ31 Alloy," *Journal of Engineering Materials and Technology*, 132 (2010), 041008-1-10.

10. H.M. Rao, J.B. Jordon, H.Badarinarayan, M.F. Hostemeyer "Effect of weld structure on fatigue life of fssw in Mg AZ31 alloys," (Paper presented at 141st Annual Meeting of TMS, Orlando, FL, March 15th 2012), 3.

11. D.L. McDowell, Ken Gall, M.F. Horstemeyer, and J. Fan. "Microstructure-Based Fatigue Modeling of Cast A356-T6 Alloy," *Engineering Fracture Mechanics*, Vol. 70, pp. 49-80, 2003.

12. Y. Xue, D.L. McDowell, M.F. Horstemeyer, M.H. Dale, and J.B. Jordon. "Microstructure-based Multisatge Fatigue Modeling of Aluminum Alloy 7075-T651," *Engineering Fracture Mechanics*, Vol. 74, Issue 17, pp. 2810-2823, 2007.

13. J.B. Jordon, J. Gibson, M.F. Horstemeyer, H. El Kadiri, J. Baird, and A.A. Luo. "Effect of Twinning, Slip, and Inclusions on the Fatigue Anisotropy of Extrusion-Textured AZ61 Magnesium Alloy," *Materials Science and Engineering A*, Vol. 528, pp. 6860– 6871, 2011.

14. S. Groh, E.B. Marin, M.F. Horstemeyer,and D.J. Bammann. "Dislocation Motion in Magnesium: A Study by Molecular Statistics and Molecular Dynamics, Modelling and Simulation," *Materials Science and Engineering*, Vol. 17, pp. 1-15, 2009.

15. Sabrina Alam Khan, Yukio Miyashita, Yoshiharu Mutoh, Zainuddin Bin Sajuri, "Influence of Mn content on mechanical properties and fatigue behavior of extruded Mg alloys," *Materials Science and Engineering A 420 (2006) 315–32.*

16. Zainuddin Bin Sajuri, Yukio Miyashita, Yasunobu Hosokai, Yoshiharu Mutoh, "Effects of Mn content and texture on fatigue properties of as-cast and extruded AZ61 magnesium alloys," *International Journal of Mechanical Sciences 48 (2006) 198–209*

17. Hiroshi Tada, Paul Paris and George Irwin, *The Stress Analysis of Cracks Handbook* (New York, NY: ASME, 2000), 40.

Appendix

Table IV. Microstructure-sensitive fatigue modeling parameters for AZ31 magnesium alloy

Constant	Parameters	Description
C_{inc}	9	Linear coefficient (Eq. 2)
α	-0.65	Ductility exponent in Modified Coffin Manson Law (Eq. 2)
X	3	Exponent in remote strain to local plastic shear strain (Eq. 3)
E	155 (MPa)	Elastic Limit
K'	494 (MPa)	Cyclic strain strength coefficient
N'	0.14	Cyclic strain hardening exponent
χ	0.28	Crack growth rate constant (Eq. 4)
C_{I}	0.00007	HCF constant in small crack growth (Eq. 5)
C_{II}	0.002	LCF constant in small crack growth (Eq. 5)
ω	2	Omega (Eq. 5)
ζ	1.2	Exponent in Small crack growth (Eq. 5)
t	2 (mm)	Sheet thickness (Eq.8 & 9)